

Chapter 4

NUMERICAL MODELING OF SPHERICAL SHELLS OF CONVECTION

4.1 NUMERICAL MODELING OF ANELASTIC FLUIDS

Observations of supergranular and larger-scale flow fields, such as those presented in Chapter 3, together with measurements of the smaller-scale patterns of mesogranulation and granulation, provide the only direct look at the turbulent motions which occupy the underlying convection zone. Such observations indicate this convection is extremely complex, forming coherent features such as networks of upflows and downflows possessing a broad range of length and time scales. These vigorous overturning motions are permeated by magnetic structures of all sizes, ranging from small flux tubes to large-scale magnetic patterns associated with active regions and sunspots observed at the surface. To investigate further the dynamics of such turbulent flows on supergranular and larger scales, we now turn to three-dimensional numerical simulations of convection occupying thin spherical shells located immediately below the solar surface.

The simulations described in the next chapter are carried out using the anelastic spherical harmonic (ASH) code. The ASH code solves the anelastic equations of hydrodynamics describing a compressible fluid confined to a rotating spherical shell heated from below. The complex structures and intricate behavior of the resulting convection requires high spatial resolution, and the flows must be studied over extended periods of time for statistical equilibration to be achieved. As a result, the ASH code is de-

signed to run efficiently on massively parallel architectures such as the Cray T3E and SGI Origin 2000 machines (Clune et al. 1999). This multi-processor version was devised by Tom Clune, Mark Miesch, and Julian Elliott, although the numerical approach to this problem was first implemented by Gary Glatzmaier in the early 1980's (Glatzmaier 1984).

The ASH code employs a pseudo-spectral approach, where all fluid velocities and state variables are projected onto orthogonal basis functions in each of the three spatial dimensions. The radial structure of the solution variables is represented by an expansion based on Chebyshev polynomials, while variations in the latitudinal and longitudinal directions are expanded over spherical harmonic basis functions Y_ℓ^m , characterized by the angular degree ℓ and azimuthal order m . This discretization scheme ensures that the horizontal resolution is uniform everywhere on a sphere when all (ℓ, m) -pairs for a given maximum degree ℓ_{\max} are retained in the modal expansion. Conversely, the simplest finite-difference scheme, where computational gridpoints are distributed along lines of latitude and longitude, suffers from the problem that the spatial resolution varies with latitude such that the gridpoints are more closely spaced near the poles compared to equatorial regions (colloquially known as the *pole problem*).

As the name implies, the ASH code solves an approximate form of the Navier-Stokes equations known as the anelastic equations. The anelastic approximation (Gough 1969) allows us to handle the effects of compressibility while filtering out acoustic perturbations which would otherwise severely limit the size of the computational time step. This approximation is valid when the convective fluid velocities are subsonic, which in turn implies that the stratification of the fluid is only slightly superadiabatic. The filtering is achieved by insisting that the time derivative of density vanishes in the continuity equation, or thereby that the divergence of the momentum be zero, or that the momentum vector be solenoidal. This approximation is effectively equivalent to allowing pressure disturbances to equilibrate instantaneously, forcing the system to evolve on

convective rather than sound-speed time scales. It is therefore implicitly assumed that sound waves do not play a significant role in the dynamical evolution of the system, which is in agreement with the expectation that the coupling of convection, stratification, and rotation are the major dynamical influences throughout the bulk of the convection zone.

As with the temporal scales of motion, fully resolving all spatial scales of motion in a numerical simulation is infeasible at this time, as the dynamically active scales in the solar convection zone range from 10^2 Mm (depth of the zone) to 10^{-4} Mm (typical dissipation scale), thereby encompassing a factor of 10^6 in scale. However, current simulations can cope with a range of only about 10^3 in each of three dimensions. Consequently, the ASH code adopts the common approach of parameterizing the transport properties resulting sub-grid scale (SGS) turbulent eddies and resolving only the largest scales of convection, thus becoming a large eddy simulation (LES).

All LES-SGS simulations require a prescription for representing the effects of SGS convective motions not explicitly resolved in the model. Such a scheme may incorporate characteristics of the resolved flows into their functional forms (see the reviews by Canuto 1996; Lesieur 1997; Canuto & Christensen-Dalsgaard 1998), or may simply enhance the molecular (viscous and thermal) diffusivities. We have adopted the latter approach for simplicity, yet recognize that this aspect requires considerable attention in the future. The main drawback of this scheme is that the enhanced diffusion draws energy from larger resolved scales of motion which should be unaffected by such dissipative effects. In one alternative approach, known as hyperviscosity, one allows the enhanced eddy diffusivities to act on fourth (or higher) order derivatives of the velocity field, thereby confining the diffusive effects more toward the smaller end of the spectrum. Another class of SGS models involves adding extra stress terms to the equations of motion. Evolution equations for these additional contributions can then be constructed once functional forms for the correlations between second-order variables are specified

using some kind of a closure hypothesis. As is true of all LES-SGS studies, one hopes that the specific form by which the SGS motions are parameterized has a relatively small effect on the global dynamics of the system.

Time-stepping in the ASH code is performed using an implicit second-order Crank-Nicholson procedure for the linear terms and a fully explicit second-order Adams-Bashforth procedure for the nonlinear terms. Because the explicit time-stepping procedure cannot be performed in the spectral domain, this scheme necessitates conversions between the physical and spectral representations during each time step when switching between solving the implicit and explicit terms in the evolution equations. However, the benefits gained by avoiding the pole problem prevalent in finite difference representations outweigh the added computational time spent in performing the transformations between the physical and spectral domains.

4.2 THE ASH CODE: EQUATION SUMMARY

4.2.1 Fluid Flow in a Rotating Frame

We first set down the equations valid for a fully compressible, rotating fluid before introducing the anelastic approximation. We choose to operate in spherical polar coordinates (r, θ, ϕ) , where r is the radius at each point, and θ and ϕ are respectively the polar (latitude) and azimuthal (longitude) angles. The fluid is rotating with respect to an inertial frame at constant angular velocity $\boldsymbol{\Omega}$, such that

$$\boldsymbol{\Omega} = \Omega \cos \theta \hat{\mathbf{r}} - \Omega \sin \theta \hat{\boldsymbol{\theta}}, \quad (4.1)$$

as illustrated in Figure 4.1. All symbols appearing in this section are defined in Table 4.1 for convenience, and most have their usual meanings in a fluid dynamical context. The fluid equations express the conservation of mass (mass continuity),

$$\frac{\partial \rho}{\partial t} + \nabla \cdot (\rho \mathbf{u}) = 0, \quad (4.2)$$

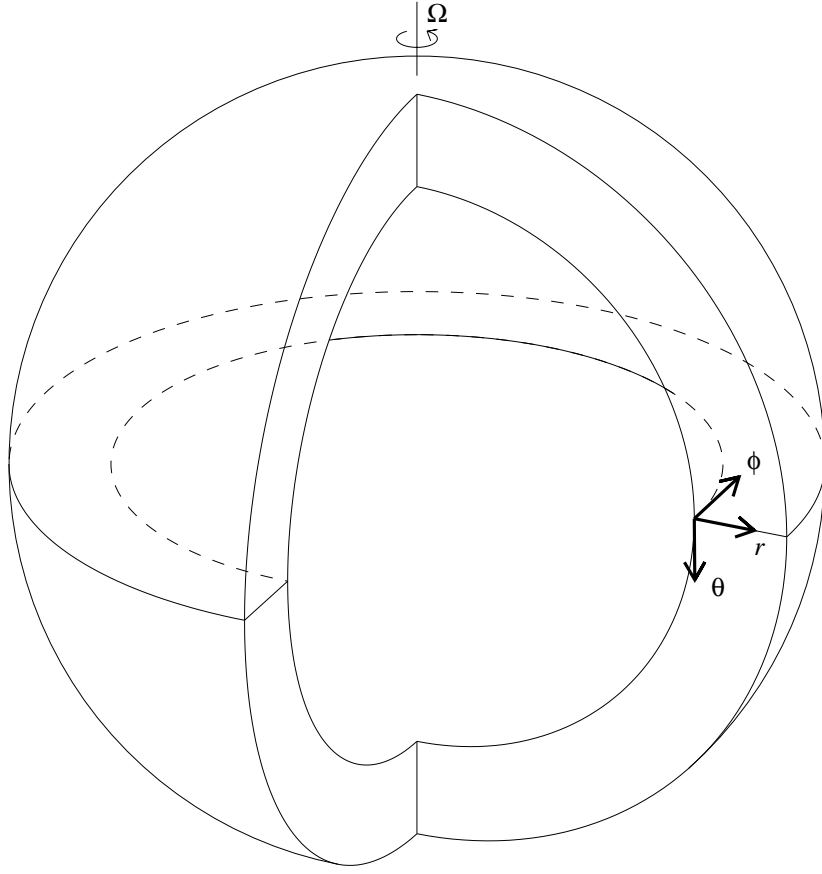


Figure 4.1: The spherical shell domain in partial cutaway to show the empty interior.

the conservation of momentum,

$$\rho \left[\frac{\partial \mathbf{u}}{\partial t} + (\mathbf{u} \cdot \nabla) \mathbf{u} \right] = -\nabla p - \rho g \hat{\mathbf{r}} + 2\rho(\mathbf{u} \times \boldsymbol{\Omega}) + \nabla \cdot \underline{\underline{\mathcal{D}}}, \quad (4.3)$$

and the conservation of internal energy,

$$\rho T \left[\frac{\partial s}{\partial t} + (\mathbf{u} \cdot \nabla) s \right] = -\nabla \cdot \mathbf{q}_{\text{eff}} + \Phi. \quad (4.4)$$

In the momentum conservation equation, it is customary for the gravitational acceleration term to contain contributions from both centrifugal acceleration and classical Newtonian gravitational acceleration. For the solar models considered here, however, the centrifugal acceleration (of order $\Omega^2 R_\odot$) is several orders of magnitude smaller than

Table 4.1: Definitions of symbols appearing in §4.2.

| Symbol | Gaussian Unit | First Appears | Definition |
|---------------------------------------|--------------------------------------|--------------------|--------------------------------------|
| c_p | erg g ⁻¹ K ⁻¹ | equation (4.8) | specific heat at constant pressure |
| c_v | erg g ⁻¹ K ⁻¹ | γ def below | specific heat at constant volume |
| $\underline{\underline{\mathcal{D}}}$ | g cm ⁻³ s ⁻¹ | equation (4.3) | viscous stress tensor |
| $\underline{\underline{\mathbf{e}}}$ | s ⁻¹ | equation (4.5) | strain rate tensor |
| g | cm s ⁻² | equation (4.3) | Newtonian gravitational acceleration |
| p | erg cm ⁻³ | equation (4.3) | pressure |
| \mathbf{q} | erg cm ⁻² s ⁻¹ | equation (4.8) | diffusive heat flux |
| \mathbf{q}_{eff} | erg cm ⁻² s ⁻¹ | equation (4.4) | effective heat flux |
| \mathbf{q}_{turb} | erg cm ⁻² s ⁻¹ | equation (4.8) | turbulent heat flux |
| r | cm | §4.2.1 intro | radius |
| $\hat{\mathbf{r}}$ | dimensionless | equation (4.3) | radial unit vector |
| s | erg g ⁻¹ K ⁻¹ | equation (4.4) | specific entropy |
| T | K | equation (4.4) | temperature |
| t | s | equation (4.2) | time |
| \mathbf{u} | cm s ⁻¹ | equation (4.2) | velocity |
| $\underline{\underline{\delta}}$ | dimensionless | equation (4.5) | Kronecker delta |
| γ | dimensionless | equation (4.10) | ratio c_p/c_v of specific heats |
| κ_r | cm ² s ⁻¹ | equation (4.8) | radiative diffusivity |
| κ_s | cm ² s ⁻¹ | equation (4.8) | turbulent thermal diffusivity |
| θ | dimensionless | §4.2.1 intro | polar angle |
| ν | cm ² s ⁻¹ | equation (4.7) | kinematic viscosity |
| ν_{eff} | cm ² s ⁻¹ | equation (4.5) | effective kinematic viscosity |
| ν_{turb} | cm ² s ⁻¹ | equation (4.7) | turbulent kinematic viscosity |
| ρ | g cm ⁻³ | equation (4.2) | density |
| Φ | erg cm ⁻² s ⁻¹ | equation (4.4) | viscous heating |
| ϕ | dimensionless | §4.2.1 intro | azimuthal angle |
| Ω | s ⁻¹ | equation (4.3) | angular velocity of reference frame |

the Newtonian gravity (of order $\frac{GM_\odot}{R_\odot^2}$), where R_\odot and M_\odot are the solar radius and mass. In order to use simple spherical harmonic expansions, we ignore centrifugal effects in these models, thereby rendering the surfaces of constant gravitational potential spherical: $\mathbf{g} = -g \hat{\mathbf{r}}$. Note that this assumption precludes Eddington-Sweet circulations (e.g. Tassoul 1978).

The viscous stress tensor $\underline{\underline{\mathcal{D}}}$ appearing in equation (4.3) is defined as

$$\underline{\underline{\mathcal{D}}} = 2\rho\nu_{\text{eff}} \left[\underline{\underline{\mathbf{e}}} - \frac{1}{3}(\nabla \cdot \mathbf{u}) \underline{\underline{\boldsymbol{\delta}}} \right], \quad (4.5)$$

while the viscous heating term Φ appearing in equation (4.4) can be written

$$\Phi = 2\rho\nu_{\text{eff}} \left[\underline{\underline{\mathbf{e}}} : \underline{\underline{\mathbf{e}}} - \frac{1}{3}(\nabla \cdot \mathbf{u})^2 \right], \quad (4.6)$$

where in both equations (4.5) and (4.6) the tensor $\underline{\underline{\mathbf{e}}}$ is the strain rate tensor and is itself a function of \mathbf{u} .

In accordance with our SGS formulation, we define the effective viscosity ν_{eff} as

$$\nu_{\text{eff}} = \nu + \nu_{\text{turb}}, \quad (4.7)$$

where ν_{turb} is the turbulent eddy viscosity which accounts for viscous transport by convective motions not formally resolved in the simulation. In the above hydrodynamic equations, the true viscosity ν has been replaced by ν_{eff} . Additionally, we also must account for the transport of heat by the SGS turbulence. We therefore define

$$\mathbf{q}_{\text{eff}} = \mathbf{q} + \mathbf{q}_{\text{turb}} = \underbrace{-\kappa_r \rho c_p \nabla T}_{\mathbf{q}} - \underbrace{\kappa_s \rho T \nabla s}_{\mathbf{q}_{\text{turb}}}, \quad (4.8)$$

where we have explicitly taken into account the smoothing out of entropy gradients by unresolved SGS motions by having the eddy thermal diffusivity κ_s acting on ∇s . Ideally, if the simulation were to resolve all relevant scales of motion, the turbulent contributions to ν_{eff} and \mathbf{q}_{eff} would be superfluous. However, fully resolved global simulations of relevance to the sun are currently unattainable.

The heat flux \mathbf{q} appearing in equation (4.8) should contain contributions from both radiative diffusion and thermal conduction. For the sun, the energy flux due to thermal conduction is much smaller than the fluxes from radiative diffusion or convection (e.g. Spitzer 1962; Hansen & Kawaler 1994) and is thus ignored in these models. Furthermore, the radiative flux is assumed to take the form of a Fick-type diffusion law,

$$\mathbf{q} = -\kappa_r \rho c_p \nabla T. \quad (4.9)$$

Equations (4.2)–(4.4) are to be solved for the following seven quantities: the four state variables ρ , p , T , s , and the three components of \mathbf{u} . However, equations (4.2)–(4.4) comprise only five independent relations. Since only two of the state variables are independent, the system is closed by first specifying an equation of state relating the state variables ρ , p , and T , and then deriving an equation for s .

In the simulations presented here, we assume the fluid is a perfect gas, thereby ignoring the effects of ionization. The equation of state is therefore

$$p = \frac{\gamma - 1}{\gamma} c_p \rho T. \quad (4.10)$$

The specific entropy is then

$$s = c_p \left(\frac{1}{\gamma} \ln p - \ln \rho \right), \quad (4.11)$$

valid to within an arbitrary constant determined by specifying the value of s given reference values of p and ρ . Equations (4.2)–(4.4), (4.10), and (4.11) now form a complete set of equations describing a compressible fluid in a spherical geometry.

4.2.2 The Anelastic Approximation

Compressibility clearly plays an important role in the dynamics of the solar convection zone, as the fluid density varies by several orders of magnitude across the layer. The density drops by a factor of approximately 100 between $0.90R_\odot$ and $0.99R_\odot$, which encompasses the upper region of the convection zone considered in this thesis. We therefore apply the anelastic approximation to the fully compressible fluid equations in order to accommodate a solar-like density stratification in our simulations. As discussed earlier, sound waves and other pressure disturbances which operate on time scales faster than the time scale of the convection are filtered out in this formulation, since including such dynamics would otherwise limit the size of the computational time step.

The main assumption of the anelastic approximation is that such temporal filtering is valid when the convective motions are subsonic, which occurs when the radial

entropy gradient responsible for driving the convection departs only slightly from the marginally stable entropy gradient (that is, when $\left|\frac{ds}{dr}\right| \ll 1$). We now estimate the degree of superadiabaticity at a given radius within the solar convection zone using simplified mixing-length arguments to estimate the heat transport of a convectively unstable parcel of fluid.

We first define the dimensionless parameter ϵ as

$$\epsilon = -\frac{\lambda}{c_p} \frac{ds}{dr}, \quad (4.12)$$

where ϵ characterizes the superadiabaticity of the fluid in terms of the entropy gradient. To make ϵ dimensionless, we normalize the entropy gradient by choosing c_p as the entropy scale and the mixing length λ as the characteristic length scale. The negative sign in equation (4.12) ensures that ϵ is positive, since superadiabatically stratified (convectively unstable) fluids have negative entropy gradients. We assume that the superadiabatic stratification $\frac{ds}{dr}$ is prescribed throughout the convection zone, even though the very motions which it supposedly drives most assuredly feed back and alter the stratification.

Now consider an isolated fluid parcel, initially in equilibrium with its surroundings, rising through the convectively unstable medium characterized by entropy gradient $\frac{ds}{dr}$. The motion of this parcel is driven by the excess heat it possesses after rising a radial distance λ . Equating the kinetic energy of the parcel with this heat excess, we have

$$\frac{\rho v^2}{2} = -\lambda \rho T \frac{ds}{dr}, \quad (4.13)$$

where v is the upward radial velocity of the parcel, and T and ρ are representative values of the temperature and density of the fluid. Solving for v and substituting the definition of ϵ from equation (4.12) into equation (4.13), we obtain

$$v = (2\epsilon c_p T)^{\frac{1}{2}}. \quad (4.14)$$

The flux of energy $F_{\text{conv}} = \frac{1}{2} \rho v^3$ carried radially outward by these convective motions is therefore equal to

$$F_{\text{conv}} = \rho (\epsilon c_p T)^{\frac{3}{2}}, \quad (4.15)$$

where factors of order unity have been omitted from our estimate. We now determine the degree of superadiabaticity ϵ necessary for convection to transport the entire solar luminosity L_{\odot} through the convection zone by equating $F_{\text{total}} = F_{\text{conv}}$, which implies

$$\frac{L_{\odot}}{4\pi r^2} = \rho (\epsilon c_p T)^{\frac{3}{2}}, \quad (4.16)$$

and solving for ϵ . We thus have

$$\epsilon = \frac{1}{c_p T} \left(\frac{L_{\odot}}{4\pi r^2 \rho} \right)^{\frac{2}{3}}. \quad (4.17)$$

We can also estimate the typical Mach number M_a achieved by these convective flows. By definition,

$$M_a = \frac{v}{c_s}, \quad (4.18)$$

where the adiabatic sound speed c_s is given by

$$c_s = \left(\frac{\gamma p}{\rho} \right)^{\frac{1}{2}}. \quad (4.19)$$

Substituting the expressions for v and c_s from equations (4.14) and (4.19) into equation (4.18) gives

$$M_a = \left(\frac{\epsilon c_p \rho T}{\gamma p} \right)^{\frac{1}{2}} = \left(\frac{\epsilon}{\gamma - 1} \right)^{\frac{1}{2}}, \quad (4.20)$$

where the last equality follows from the ideal gas law, equation (4.10). Equation (4.20) implies that convective motions driven by a fluid for which ϵ is small do not approach the speed of sound.

Table 4.2 lists values for v , ϵ , and M_a calculated using equations (4.14), (4.17), and (4.20) for several radii within the convection zone. Values for T and ρ are taken from

Table 4.2: Estimates of v , ϵ , and M_a using a mixing-length approach as calculated from equations (4.14), (4.17), and (4.20) assuming $L_\odot = 3.90 \times 10^{33}$ erg s $^{-1}$, $R_\odot = 6.96 \times 10^{10}$ cm, and $c_p = 4 \times 10^8$ erg g $^{-1}$ K $^{-1}$. The temperature T and density ρ are taken from Model S of Christensen-Dalsgaard et al. (1993). In this model, the base of the convection zone sits at $r = 0.73R_\odot$.

| $r [R_\odot]$ | T [K] | ρ [g cm $^{-3}$] | v [m s $^{-1}$] | ϵ | M_a |
|---------------|-------------------|------------------------|--------------------|--------------------|--------------------|
| 0.73 | 2.1×10^6 | 1.6×10^{-1} | 130 | 1×10^{-7} | 4×10^{-4} |
| 0.75 | 1.8×10^6 | 1.3×10^{-1} | 140 | 1×10^{-7} | 4×10^{-4} |
| 0.80 | 1.4×10^6 | 8.8×10^{-2} | 150 | 2×10^{-7} | 5×10^{-4} |
| 0.85 | 9.9×10^5 | 5.2×10^{-2} | 170 | 4×10^{-7} | 7×10^{-4} |
| 0.90 | 6.2×10^5 | 2.6×10^{-2} | 200 | 8×10^{-7} | 1×10^{-3} |
| 0.94 | 3.5×10^5 | 1.0×10^{-2} | 270 | 3×10^{-6} | 2×10^{-3} |
| 0.96 | 2.2×10^5 | 5.3×10^{-3} | 330 | 6×10^{-6} | 3×10^{-3} |
| 0.97 | 1.6×10^5 | 3.1×10^{-3} | 400 | 1×10^{-5} | 4×10^{-3} |
| 0.98 | 1.0×10^5 | 1.4×10^{-3} | 510 | 3×10^{-5} | 7×10^{-3} |
| 0.99 | 4.7×10^4 | 3.2×10^{-4} | 830 | 2×10^{-4} | 2×10^{-2} |
| 0.999 | 1.3×10^4 | 1.2×10^{-6} | 5300 | 3×10^{-2} | 2×10^{-1} |

an advanced one-dimensional solar model used extensively in helioseismology (Model S of Christensen-Dalsgaard et al. 1993). Table 4.2 shows that ϵ is no greater than about 10^{-4} (and thus $M_a \lesssim 10^{-2}$) throughout the bulk of the convection zone, and so the convective motions driven at greater depths are expected to be decidedly subsonic. Only within the last 1% by radius does ϵ approach unity. Above $0.99R_\odot$, the rapidly decreasing density and temperature profiles lead to faster fluid motions involving smaller spatial and temporal scales. In addition, the recombination of electrons with helium and hydrogen nuclei release latent heat which then must be transported outward by the convection. As a result, the stratification must become more superadiabatic to transport the requisite amount of energy, rendering the anelastic approximation less valid.

4.2.3 Scaling of the Fully Compressible Fluid Equations

Because the convective motions are subsonic and the superadiabaticity within the convection zone is small, we expect that the resulting departures of the thermodynamic

state variables from their spherically averaged means should also be small. Therefore, we perform a formal scale analysis on the fully compressible fluid equations (4.2)–(4.4) introduced in §4.2.1 to separate the spherically symmetric mean state from the fluctuations resulting from the convection. We express each state variable f as the sum of a spherically symmetric mean quantity $\hat{f}(r, t)$ and a fluctuating quantity $f'(r, \theta, \phi, t)$:

$$\begin{aligned}
 p(r, \theta, \phi, t) &= \hat{p}(r, t) + p'(r, \theta, \phi, t), \\
 \rho(r, \theta, \phi, t) &= \hat{\rho}(r, t) + \rho'(r, \theta, \phi, t), \\
 T(r, \theta, \phi, t) &= \hat{T}(r, t) + T'(r, \theta, \phi, t), \\
 s(r, \theta, \phi, t) &= \hat{s}(r, t) + s'(r, \theta, \phi, t).
 \end{aligned}
 \tag{4.21}$$

The perturbations to the state variables result from convective motions driven by the superadiabatic stratification of the layer, which we have previously characterized by the parameter ϵ defined in equation (4.12). We therefore assume $\frac{f'}{\hat{f}}$ is of order ϵ for any quantity f in equation (4.21).

For low Mach number flows the time scale on which pressure and density perturbations get smoothed out is much faster than the time scale of the convective motions, since such perturbations dissipate on sound-speed time scales. We perform such temporal filtering by assuming

$$\frac{\partial \rho'}{\partial t} = 0
 \tag{4.22}$$

in the mass continuity equation.

The resulting anelastic equations consist of a set of equations describing the mean state, and a system of dynamic equations which governs the evolution of the fluctuating quantities. The details of the formal scale separation, which include the derivations of equations (4.23)–(4.33) which follow, are presented in §B.1 of Appendix B. We assume that the diffusivities ν_{eff} , κ_r , and κ_s are functions of $\hat{\rho}$ (and thus r) only, while the parameters γ and c_p are assumed constant throughout the domain.

The mean momentum equation becomes

$$\frac{d(\hat{p} + \hat{p}_{\text{turb}})}{dr} = -\hat{\rho}g, \quad (4.23)$$

where the quantity $\hat{p}_{\text{turb}}(r, t)$ represents the small departure from hydrostatic equilibrium caused by the combined effect of turbulent motions in the system. The mean equations of state are

$$\hat{p} = \frac{\gamma - 1}{\gamma} c_p \hat{\rho} \hat{T}, \quad (4.24)$$

$$\frac{d\hat{s}}{dr} = c_p \left(\frac{1}{\gamma \hat{p}} \frac{d\hat{p}}{dr} - \frac{1}{\hat{\rho}} \frac{d\hat{\rho}}{dr} \right). \quad (4.25)$$

Upon initialization, the equations (4.23)–(4.25) are solved to determine the mean state, with the turbulent pressure $\hat{p}_{\text{turb}} = 0$ since the system is started from rest. Because there are only three equations but four unknown mean variables, one of them is therefore undetermined. Consequently, we take the approach of prescribing the entropy gradient $\frac{d\hat{s}}{dr}$, and then solving equations (4.23)–(4.25) to determine the other mean variables \hat{p} , $\hat{\rho}$, and \hat{T} . Note that the gravitational acceleration g can either be assumed constant throughout the layer, or can be prescribed along with the entropy gradient if the self-gravity of the mean state is deemed important.

The equations governing the evolution of the dynamic quantities \mathbf{u} and s are:

$$\hat{\rho} \frac{\partial \mathbf{u}}{\partial t} = 2\hat{\rho}(\mathbf{u} \times \boldsymbol{\Omega}) - \hat{\rho}(\mathbf{u} \cdot \nabla)\mathbf{u} - \nabla p' - \rho' g \hat{\mathbf{r}} + \nabla \cdot \hat{\underline{\underline{\mathcal{D}}}} \quad (4.26)$$

and

$$\hat{\rho} \hat{T} \frac{\partial s'}{\partial t} = \nabla \cdot \hat{\mathbf{q}}_{\text{eff}} - \hat{\rho} \hat{T} (\mathbf{u} \cdot \nabla)(\hat{s} + s') + \hat{\Phi}, \quad (4.27)$$

where the anelastic viscous stress tensor $\hat{\underline{\underline{\mathcal{D}}}}$ and the anelastic viscous heating term $\hat{\Phi}$ are defined

$$\hat{\underline{\underline{\mathcal{D}}}} = 2\hat{\rho} \nu_{\text{eff}} \left[\underline{\underline{\mathbf{e}}} - \frac{1}{3} (\nabla \cdot \mathbf{u}) \underline{\underline{\delta}} \right] \quad (4.28)$$

and

$$\hat{\Phi} = 2\hat{\rho}\nu_{\text{eff}} \left[\underline{\underline{\mathbf{e}}} : \underline{\underline{\mathbf{e}}} - \frac{1}{3}(\nabla \cdot \mathbf{u})^2 \right], \quad (4.29)$$

and where the anelastic heat flux $\hat{\mathbf{q}}_{\text{eff}}$ is defined as

$$\hat{\mathbf{q}}_{\text{eff}} = -\kappa_r \hat{\rho} c_p \nabla(\hat{T} + T') - \kappa_s \hat{\rho} \hat{T} \nabla(\hat{s} + s'). \quad (4.30)$$

The evolution of the system given by equations (4.26)–(4.27) are subject to the following three constraints:

$$\nabla \cdot (\hat{\rho} \mathbf{u}) = 0, \quad (4.31)$$

$$\frac{p'}{\hat{p}} = \frac{\rho'}{\hat{\rho}} + \frac{T'}{\hat{T}}, \quad (4.32)$$

$$\frac{s'}{c_p} = \frac{p'}{\gamma \hat{p}} - \frac{\rho'}{\hat{\rho}}. \quad (4.33)$$

4.2.4 Energetics of the Anelastic Equations

For future reference, we now list the equations describing the kinetic and internal energy budgets of the system, while relegating the detailed derivations to §B.2 in Appendix B. The equation describing the conservation of kinetic energy density $\mathcal{E}_k = \frac{\hat{\rho} \mathbf{u} \cdot \mathbf{u}}{2}$ is

$$\frac{\partial \mathcal{E}_k}{\partial t} = -\mathbf{u} \cdot \nabla p' - \rho' g \mathbf{u} \cdot \hat{\mathbf{r}} + \mathbf{u} \cdot (\nabla \cdot \hat{\underline{\underline{\mathcal{D}}}}) + \nabla \cdot \left[\mathbf{u} \left(\frac{\hat{\rho} \mathbf{u} \cdot \mathbf{u}}{2} \right) \right]. \quad (4.34)$$

The terms on the right-hand side of equation (4.34) all represent sources or sinks of kinetic energy due to work respectively done by pressure gradient forces, buoyancy forces, shear stresses, and by inertial forces.

The equation describing the conservation of internal energy density $\mathcal{E}_s = \hat{\rho} \hat{T} s'$ is

$$\frac{\partial \mathcal{E}_s}{\partial t} = \nabla \cdot \hat{\mathbf{q}}_{\text{eff}} + \mathbf{u} \cdot \nabla p' + \rho' g \mathbf{u} \cdot \hat{\mathbf{r}} - c_p \nabla \cdot (\hat{\rho} T' \mathbf{u}) + \hat{\Phi}. \quad (4.35)$$

As with the kinetic energy equation, each of the terms on the right-hand side of equation (4.35) represents either a source or sink of internal energy. The first term on

the right-hand side represents the transport of flux via temperature/entropy gradients throughout the domain. The next two terms denote the extraction of heat from the thermal field by pressure-gradient and buoyancy forces. The fourth and fifth terms represent the heat generated by volume expansion and viscous dissipation, while the sixth term may be interpreted as the radial transport of enthalpy.

The sum of equations (4.34) and (4.35) yields the following equation describing the total energy budget of the system:

$$\frac{\partial(\mathcal{E}_k + \mathcal{E}_s)}{\partial t} = \nabla \cdot (\mathbf{u} \cdot \underline{\hat{\mathcal{D}}}) + \nabla \cdot \left[\mathbf{u} \left(\frac{\hat{\rho} \mathbf{u} \cdot \mathbf{u}}{2} \right) \right] + \nabla \cdot \hat{\mathbf{q}}_{\text{eff}} - \nabla \cdot (c_p \hat{\rho} T' \mathbf{u}). \quad (4.36)$$

4.2.5 Streamfunction Formalism

To solve the anelastic evolution equations (4.26) and (4.27), we recognize that the mass flux is solenoidal, which permits the quantity $\hat{\rho} \mathbf{u}$ to be written in terms of poloidal and toroidal streamfunctions W and Z ,

$$\hat{\rho} \mathbf{u} = \nabla \times (\nabla \times W \hat{\mathbf{r}}) + \nabla \times Z \hat{\mathbf{r}} \quad (4.37)$$

such that equation (4.31) is automatically satisfied. We now replace the anelastic momentum equation (4.26) with three scalar equations describing the evolution of W , $\frac{\partial W}{\partial r}$, and Z . They are the radial component of the momentum equation,

$$-\frac{\partial}{\partial t}(\nabla_{\perp}^2 W) = -\frac{\partial p'}{\partial r} - \hat{\rho} g + \hat{\mathbf{r}} \cdot [\nabla \cdot \underline{\hat{\mathcal{D}}}] + \hat{\rho} \hat{\mathbf{r}} \cdot [2(\mathbf{u} \times \boldsymbol{\Omega}) - (\mathbf{u} \cdot \nabla) \mathbf{u}], \quad (4.38)$$

the horizontal divergence of the momentum equation,

$$-\frac{\partial}{\partial t} \left[\frac{\partial}{\partial r} (\nabla_{\perp}^2 W) \right] = -\nabla_{\perp}^2 p' + \nabla_{\perp} \cdot [\nabla \cdot \underline{\hat{\mathcal{D}}}] + \hat{\rho} \nabla_{\perp} \cdot [2(\mathbf{u} \times \boldsymbol{\Omega}) - (\mathbf{u} \cdot \nabla) \mathbf{u}], \quad (4.39)$$

and the radial component of the curl of the momentum equation,

$$\begin{aligned} -\frac{\partial}{\partial t}(\nabla_{\perp}^2 Z) &= \hat{\mathbf{r}} \cdot [\nabla \times (\nabla \cdot \underline{\hat{\mathcal{D}}})] - \hat{\rho} \hat{\mathbf{r}} \cdot [\nabla \times (\mathbf{u} \cdot \nabla) \mathbf{u}] \\ &\quad + 2(\boldsymbol{\Omega} \cdot \nabla) \hat{\rho} u_r + \frac{2\hat{\rho} \Omega u_{\theta} \sin \theta}{r}. \end{aligned} \quad (4.40)$$

In the above equations, the horizontal Laplacian operator is defined

$$\nabla_{\perp}^2 = \frac{1}{r^2 \sin \theta} \frac{\partial}{\partial \theta} \left(\sin \theta \frac{\partial}{\partial \theta} \right) + \frac{1}{r^2 \sin^2 \theta} \frac{\partial^2}{\partial \phi^2}, \quad (4.41)$$

while the horizontal divergence of a vector \mathbf{A} is defined

$$\nabla_{\perp} \cdot \mathbf{A} = \frac{1}{r \sin \theta} \frac{\partial(\sin \theta A_{\theta})}{\partial \theta} + \frac{1}{r \sin \theta} \frac{\partial A_{\phi}}{\partial \phi}. \quad (4.42)$$

Equations (4.38)–(4.40), together with the anelastic energy equation (4.27), form the evolution equations solved by the ASH code. Detailed derivations of these equations are provided in §B.3 of Appendix B.

4.3 THE ASH CODE: NUMERICAL IMPLEMENTATION

We now summarize the discretization scheme and parallel implementation of the ASH code, following the more detailed presentation of Miesch (1998).

4.3.1 Angular Discretization

The first step in the pseudo-spectral method is to express all dependent variables as a projection over orthogonal basis functions. For the angular dependence, the basis functions are the spherical harmonics Y_{ℓ}^m ,

$$Y_{\ell}^m(\theta, \phi) = C_{\ell}^m P_{\ell}^m(\cos \theta) e^{im\phi}, \quad (4.43)$$

where the functions P_{ℓ}^m are the associated Legendre functions, and where the constants C_{ℓ}^m are defined

$$C_{\ell}^m = (-1)^m \left[\frac{2\ell + 1}{4\pi} \frac{(\ell - m)!}{(\ell + m)!} \right]^{\frac{1}{2}}. \quad (4.44)$$

The spherical harmonic functions are characterized by the angular degree ℓ and azimuthal order m . All dependent variables $f(r, \theta, \phi, t)$ in the problem are expressed as linear combinations of the spherical harmonics,

$$f(r, \theta, \phi, t) = \sum_{\ell=0}^{\infty} \sum_{m=-\ell}^{\ell} f_{\ell}^m(r, t) Y_{\ell}^m(\theta, \phi), \quad (4.45)$$

where the spectral coefficients $f_\ell^m(r, t)$ are found by the formula

$$\begin{aligned} f_\ell^m(r, t) &= \int_0^{2\pi} d\phi \int_0^\pi \sin \theta d\theta Y_\ell^{m*}(\theta, \phi) f(r, \theta, \phi, t) \\ &= C_\ell^m \int_0^\pi \sin \theta d\theta P_\ell^m(\cos \theta) \int_0^{2\pi} d\phi e^{-im\phi} f(r, \theta, \phi, t). \end{aligned} \quad (4.46)$$

Equation (4.46) constitutes the continuous spherical harmonic transform formula.

Numerical simulations are of course discretized, either by having a discrete grid in physical space or by limiting the number of mode coefficients in spectral space. To maximize the accuracy of the transforms, Gaussian quadrature techniques are utilized in evaluating the integrals of equation (4.46), where continuous integrals are approximated as weighted sums over predetermined collocation points (θ_i, ϕ_j) known as Gaussian abscissae. The Gaussian abscissae depend only on the number of collocation points and the orthogonal basis used in the expansion. Using Gaussian quadrature, the spherical harmonic transform of equation (4.46) becomes

$$\begin{aligned} f_\ell^m(r, t) &= C_\ell^m \sum_{i=1}^{N_\theta} w_i P_\ell^m(\cos \theta_i) \sum_{j=1}^{N_\phi} w_j e^{-im\phi_j} f(r, \theta_i, \phi_j, t) \\ &= \sum_{i=1}^{N_\theta} \sum_{j=1}^{N_\phi} w_i w_j Y_\ell^{m*}(\theta_i, \phi_j) f(r, \theta_i, \phi_j, t), \end{aligned} \quad (4.47)$$

where N_θ and N_ϕ are the number of collocation points used in the θ and ϕ directions. In this formula, the Gaussian abscissae in ϕ are the Fourier collocation points ϕ_j , where

$$\phi_j = \frac{2\pi j}{N_\phi} \quad \text{where} \quad j = 1, 2, \dots, N_\phi, \quad (4.48)$$

having weights w_j of

$$w_j = \frac{1}{N_\phi}. \quad (4.49)$$

The Gaussian abscissae in θ are the Legendre collocation points θ_i , where

$$\theta_i = \text{zeroes of } P_{N_\theta}(\cos \theta) \quad \text{with} \quad i = 1, 2, \dots, N_\theta, \quad (4.50)$$

having weights w_i of

$$w_i = \frac{2}{[\sin^2 \theta_i P'_{N_\theta}(\cos \theta_i)]^2}. \quad (4.51)$$

In equations (4.50) and (4.51), the functions $P_\ell(\cos \theta)$ are the Legendre functions of the first kind, with

$$P'_{N_\theta} = \left. \frac{dP_{N_\theta}(\cos \theta)}{d(\cos \theta)} \right|_{\theta=\theta_i}. \quad (4.52)$$

The values N_θ and N_ϕ determine the angular resolution in physical space in both the latitudinal and longitudinal directions. To ensure that the horizontal resolution is even everywhere on a spherical surface, we set $N_\phi = 2N_\theta$, and truncate the spherical harmonic expansion of equation (4.45) at a maximum angular degree ℓ_{\max} , wherein all modes for which $0 \leq \ell \leq \ell_{\max}$ and $-\ell_{\max} \leq m \leq \ell_{\max}$ are used in the expansion. To attenuate aliasing errors when evaluating the nonlinear terms in the evolution equations, we also choose ℓ_{\max} to satisfy

$$N_\theta \geq \frac{3\ell_{\max} + 1}{2}. \quad (4.53)$$

4.3.2 Radial Discretization

As with the angular discretization, the radial discretization is handled in a similar fashion. The radial dependence of each field is evaluated only at discrete collocation points, and is transformed to spectral space using Gaussian quadrature. Each coefficient $f_\ell^m(r, t)$ is expanded over the set of Chebyshev polynomials T_n of order n , where

$$T_n(x) = \cos(n \arccos x). \quad (4.54)$$

While the T_n appear trigonometric, they are in fact polynomials in x defined on $(-1, 1)$.

The physical radii r_k are scaled to the Chebyshev gridpoints x_k by

$$r_k = \frac{1}{2} \left[(r_1 + r_2) + (r_2 - r_1)x_k \right], \quad (4.55)$$

where r_1 and r_2 are respectively the radii of the lower and upper boundary of the physical domain such that they map to -1 and 1 in the Chebyshev domain.

Each discrete function $f_\ell^m(r_k, t)$ can be expressed as a truncated series

$$f_\ell^m(r_k, t) = \frac{2}{N_r - 1} \sum_{n=1}^{N_r} \epsilon_n f_{\ell n}^m(t) T_{n-1}(x_k), \quad (4.56)$$

where the spectral coefficients $f_{\ell n}^m$ are found by evaluating

$$f_{\ell n}^m = \sum_{k=1}^{N_r} w_k T_{n-1}(x_k) f_\ell^m(x_k, t). \quad (4.57)$$

The Chebyshev collocation points x_k are

$$x_k = \cos\left(\frac{(k-1)\pi}{N_r - 1}\right), \quad (4.58)$$

while the weights w_k are

$$w_k = \frac{\epsilon_k \pi}{N_r - 1}. \quad (4.59)$$

In this formula and in equation (4.56), the constant ϵ_k is equal to 1, unless $k = 1$ or $k = N_r$, for which $\epsilon_k = \frac{1}{2}$.

4.3.3 Temporal Discretization and Parallel Implementation

When transformed to spectral space, the ASH code evolution equations (4.27) and (4.38)–(4.40) are of the form

$$\frac{\partial y}{\partial t} = \mathcal{L} + \mathcal{N}, \quad (4.60)$$

where \mathcal{L} and \mathcal{N} respectively designate linear and nonlinear source terms.¹ Generally, these source terms can be a function of any of the dependent variables W , Z , p , and s as well as a function of the independent variables r , θ , ϕ , and t .

The time-stepping for both the linear and nonlinear source terms is performed simultaneously using a combination of the Crank-Nicholson scheme for the linear source

¹ Although the Coriolis terms are linear, they are grouped with the nonlinear source terms \mathcal{N} in the ASH code time-stepping algorithm.

terms \mathcal{L} and the Adams-Bashforth scheme for the nonlinear source terms \mathcal{N} . Both methods are accurate to second-order. By combining the two methods (see Appendix C), we discretize equation (4.60) to obtain

$$\frac{y_{i+1} - y_i}{\Delta t_i} = \left(1 + \frac{1}{2} \frac{\Delta t_i}{\Delta t_{i-1}}\right) \mathcal{N}_i - \left(\frac{1}{2} \frac{\Delta t_i}{\Delta t_{i-1}}\right) \mathcal{N}_{i-1} + \Theta \mathcal{L}_{i+1} + (1 - \Theta) \mathcal{L}_i, \quad (4.61)$$

where subscripts are used to denote the index of the time step. For example, y_i denotes the value of y at the most recently computed time step (occurring at time t_i) and y_{i+1} denotes the yet-to-be-computed value of y at the next time step. The time separation between subsequent time steps is $\Delta t_i = t_{i+1} - t_i$.

After rewriting, equation (4.61) becomes

$$y_{i+1} - \Delta t_i \Theta \mathcal{L}_{i+1} = y_i + \Delta t_i \left[\left(1 + \frac{1}{2} \frac{\Delta t_i}{\Delta t_{i-1}}\right) \mathcal{N}_i - \left(\frac{1}{2} \frac{\Delta t_i}{\Delta t_{i-1}}\right) \mathcal{N}_{i-1} + (1 - \Theta) \mathcal{L}_i \right]. \quad (4.62)$$

Since the term \mathcal{L}_{i+1} is linear, we may write $\mathcal{L}_{i+1} = \mathcal{A}' y_{i+1}$, where \mathcal{A}' is a matrix operator.

Equation (4.62) now becomes the matrix equation

$$\mathcal{A} y_{i+1} = \mathcal{B}, \quad (4.63)$$

where

$$\mathcal{A} = 1 - \Delta t_i \Theta \mathcal{A}' \quad (4.64)$$

and

$$\mathcal{B} = y_i + \Delta t_i \left[\left(1 + \frac{1}{2} \frac{\Delta t_i}{\Delta t_{i-1}}\right) \mathcal{N}_i - \left(\frac{1}{2} \frac{\Delta t_i}{\Delta t_{i-1}}\right) \mathcal{N}_{i-1} + (1 - \Theta) \mathcal{L}_i \right]. \quad (4.65)$$

The updated fields y_{i+1} are determined by solving the matrix equation (4.63) once \mathcal{A} and \mathcal{B} are calculated.

We now summarize the main loop of the ASH code:

- At the beginning of each iteration, the dependent variables y_i begin in (r, ℓ, m) -space.

- Spatial derivatives of the dependent variables are evaluated. First, each quantity is transformed to (n, ℓ, m) -space via a Chebyshev transform, then the derivatives are evaluated using Chebyshev recursion relations, and then the derivatives are transformed back to (r, ℓ, m) -space via an inverse Chebyshev transform.
- The linear term \mathcal{L}_i is evaluated in (r, ℓ, m) -space.
- The dependent variables y_i are transformed to (r, θ, ϕ) -space via an inverse Legendre transform (to go from ℓ to θ) and an inverse Fourier transform (to go from m to ϕ).
- The nonlinear term \mathcal{N}_i is evaluated in (r, θ, ϕ) -space.
- The nonlinear term \mathcal{N}_i is transformed back to (r, ℓ, m) -space via a forward Legendre transform and a forward Fourier transform.
- The quantity \mathcal{B} of equation (4.65) is evaluated, now that we have available the terms \mathcal{L}_i , \mathcal{N}_i , and \mathcal{N}_{i-1} , with the latter term saved over from the previous time step.
- The quantity \mathcal{A} of equation (4.64) is calculated.
- The matrix equation (4.63) is solved for y_{i+1} using LU-decomposition.

As stated at the beginning of this chapter, the ASH code runs efficiently on massively parallel architectures such as the Cray T3E and Origin 2000 machines (Clune et al. 1999). These machines are of the distributed-memory configuration, where each processor has its own local memory bank independent of the other processors. Such a configuration requires to the programmer to devise sensible algorithms responsible for evenly splitting up the workload (load-balancing) and coordinating interprocessor communication when information is needed by multiple processors.

The most computationally intensive steps of the flowchart above involve global operations such as the spectral transforms and the solution of the matrix equation. The strategy adopted by the ASH code is to perform all transforms between the physical and spectral domains in-processor so as to avoid interprocessor communication during the transform. However, such a scheme requires frequent global transposes in order to arrange the data such that the dimension of the transform is local.